DRAG REDUCTION CHARACTERIZATION OF SPRAY-ON SUPERHYDROPHOBIC SURFACES IN A TURBULENT CHANNEL FLOW

Parth Khokhani
Department of Mechanical Engineering
University of Michigan
Ann Arbor, MI, USA
kparth@umich.edu

Bozhong Zhuang
Department of Materials Science and Engineering
University of Michigan
Ann Arbor, MI, USA
bozhongz@umich.edu

Fai-Wei Wang
Department of Chemical Engineering
University of Michigan
Ann Arbor, MI, USA
fweiwang@umich.edu

Harish Ganesh
Department of Naval Architecture and Marine Engineering
University of Michigan
Ann Arbor, MI, USA
gharish@umich.edu

Matthew Bross
Applied Research Laboratory
The Pennsylvania State University
University Park, PA, USA
mqb6401@psu.edu

Anish Tujeta
Department of Materials Science and Engineering
University of Michigan
Ann Arbor, MI, USA
atuteja@umich.edu

Steven Ceccio
Department of Mechanical Engineering
University of Michigan
Ann Arbor, MI, USA
ceccio@umich.edu

ABSTRACT

For marine vessels, skin friction is the dominant source of energy loss, responsible for more than 50% of total fuel consumption. Although numerous active and passive methods have been studied to mitigate this energy loss, Spray-on SuperHydrophobic Surface (SHS) are viable candidate to achieve drag reduction (DR) due to their ease of application, has shown great potential in terms of both effectiveness and cost efficiency (Golovin et al. (2016)). SHSs traps a thin air layer near the surface structures, inducing slip velocity in flow and thereby reducing drag. DR depends upon different surface and flow properties, such as Reynold number (Re), RMS roughness, solid fraction, Wenzel roughness, and so on. In this study, drag characteristics of several SHS fabricated with Fluorinated Silica NanoParticles (FSNP) and Fluoroalkyl Polyhedral Oligomeric Silsesquioxane (FPOSS) are tested in a turbulent channel flow and a boundary layer flow on a flat plate. In addition, the effect of pressure and water gas content is also studied. Finally, a relationship between observed drag reduction and SHS surface parameters under different flow conditions is proposed.

Introduction

Skin-friction drag experienced by hulls and other immersed surfaces represents a significant component of the hydrodynamic resistance encountered by marine vehicles, thereby strongly influencing fuel consumption and operating costs. Because commercial ships operate over long distances and extended durations, even small reductions in skin-friction drag can translate into significant fuel savings and lower greenhouse gas emissions. Consequently, considerable research efforts have focused on developing strategies to reduce near-wall turbulent dissipation and drag.

The reduction of hydrodynamic skin-friction drag has long been a central topic in fluid mechanics research. Numerous active flow-control approaches, such as polymer and air/bubble injection (Bushnell & Moore, 1991; Ceccio, 2010; SANDERS *et al.*, 2006), boundary layer suction and blowing (KAMETANI & FUKAGATA, 2011; Li *et al.*, 2022), plasma-based actuation (Zheng *et al.*, 2023), and active wall oscillation or motion (Kang & Choi, 2000), have shown considerable potential in decreasing turbulent drag. However, such methods require continuous energy or mass input, limiting their applicability in large-scale or long-duration marine contexts. Passive drag-reduction methods, on the other hand, modify the surface properties to manipulate the near-wall flow without requiring external energy input, making them a practical alternative for improving hydrodynamic efficiency (Golovin *et al.*, 2016).

Among passive drag-reduction approaches, surfaces with geometric features have been widely investigated. Riblets (Rastegari & Graham, 2018) and compliant surfaces (Choi *et al.*, 1997) can modify turbulence structures within the boundary layer and thereby reduce wall drag. However, the practical implementation of such surfaces over large marine structures remains challenging because of fabrication difficulty, maintenance requirements, and cost. Superhydrophobic surfaces (SHSs) provide a different mechanism for passive drag reduction by sustaining a thin layer of trapped air at the liquid–solid interface, producing a heterogeneous boundary condition composed of alternating slip and no-slip regions. The trapped air layer decreases the effective contact area between the liquid and the wall, leading to a reduction in local shear stress. SHSs are generally identified by apparent contact angles greater than 150° and small contact-angle hysteresis, characteristics associated with the Cassie–Baxter wetting regime. Whereas riblets reduce drag by allowing streamwise slip along grooves, SHSs reduce drag through the presence of a plastron that alters the interfacial flow condition (Park *et al.*, 2021).

The hydrodynamic effect of SHSs can be expressed in terms of an effective slip boundary condition,

$$u_s = \lambda_x \frac{\partial U}{\partial y} \quad (1)$$

$$v_s = 0 \quad (2)$$

$$w_s = \lambda_z \frac{\partial w}{\partial y} \quad (3)$$

where u_s,v_s, and w_s are the slip velocities in the streamwise, wall-normal, and spanwise directions, respectively, and λ_x and λ_z denote the corresponding slip lengths. Slip in the streamwise direction is generally beneficial for reducing skin-friction drag, while slip in the spanwise direction may either provide little benefit or even increase drag depending on the flow conditions (Min & Kim, 2004). In the case of randomly textured superhydrophobic surfaces, the overall or effective slip length is governed by the interplay between the fraction of surface area occupied by trapped air and the details of the underlying roughness geometry.

Although superhydrophobic surfaces have been shown to produce significant drag reduction in laminar flow regimes (Ems *et al.*, 2021; Mei & Guo, 2018; Rothstein, 2010; Tomlinson *et al.*, 2023), maintaining such benefits under turbulent conditions remains considerably more difficult. Only a few studies report sustained and spatially extended drag-reduction effects in turbulent flows (Golovin *et al.*, 2016; Gose *et al.*, 2018; Park *et al.*, 2021). In these cases, the overall drag performance of SHSs is determined by a competition between reduced skin friction due to interfacial slip and additional form drag arising from flow interaction with wetted surface asperities. This balance becomes increasingly unfavorable at higher Reynolds numbers, where the thinning viscous sublayer enhances the influence of surface roughness and can diminish net drag reduction (Gose *et al.*, 2018).

In this study, we investigate the drag-reduction performance of spray-on superhydrophobic surfaces (SHSs) in both turbulent channel flow and turbulent boundary layer flow, over channel-flow Reynolds numbers of $Re_H = 10000$–$55,000$ (corresponding friction Reynolds number $Re_\tau = 300 - 1400$) and boundary-layer Reynolds numbers of $Re_x = 10^6$–1.3×10^7 (corresponding to $Re_\tau = 1000 - 5800$). The surfaces are fabricated using fluorinated silica nanoparticles (FSNP) and fluoroalkyl polyhedral oligomeric silsesquioxane (FPOSS), with the spray pressure systematically varied to generate distinct surface morphologies and roughness characteristics. Drag reduction is quantified using pressure-drop measurements in channel flow and measured directly with load cell in boundary layer flow, with all results benchmarked against hydrodynamically smooth reference conditions. Since hydrostatic pressure can strongly influence plastron stability and thereby impact both performance and durability, selected high-performing surfaces are further examined under varying pressure conditions. In addition, experiments are conducted in channel flow across different dissolved oxygen levels to explore the coupled effects of gas solubility and pressure on plastron retention and drag-reduction effectiveness. To assess long-term robustness under sustained turbulent force, longevity tests exceeding eight hours at fixed Reynolds number are performed in channel flow and three hours in boundary layer flow to evaluate plastron stability and performance persistence.

METHOD AND APPROACH

The drag-reducing superhydrophobic surfaces (SHSs) were prepared by spray coating stainless steel substrates with a hydrophobic liquid mixture consisting of fluorinated silica nanoparticles (FSNP) as the filler, ethyl-cyanoacrylate as the binder, and a fluorinated solvent (Vertrel™ XF). The FSNPs, rendered hydrophobic through surface treatment, cluster during deposition to form hierarchical surface roughness that promotes water repellency. Ethyl-cyanoacrylate, a strong adhesive widely used in commercial cyanoacrylate ("superglue") formulations, provides mechanical integrity by firmly anchoring the nanoparticles to the substrate, thereby enhancing resistance to high shear and pressure loads typical of turbulent flow environments. The fluorinated solvent, characterized by low surface tension and high volatility, facilitates uniform particle dispersion during spraying and evaporates rapidly, minimizing runoff and ensuring consistent coating formation.

The coating formulation was kept at 1.23% FSNP and 0.61% binder, while surface wettability and drag-reduction characteristics were primarily tuned by varying spray conditions to control the resulting surface roughness. A computer-controlled spray system was employed to ensure repeatable and spatially uniform deposition, with the spray air pressure varied between 10 and 55 kPa to produce a series of surface variants (v0–v3). Lower spray pressures were not accessible due to equipment limitations. The resulting roughness characteristics of each coating are summarized in Table 1.

For comparison purposes, two additional SHS configurations were also examined. The first was a commercially available coating, NeverWet™ (Rust-Oleum Inc.), applied following the manufacturer's recommended procedure. The second was a laboratory-prepared formulation in which FSNP was replaced with fluoroalkyl polyhedral oligomeric silsesquioxane (FPOSS), a commonly used fluorinated compound. This FPOSS-based coating was deposited using the same spray parameters as the v2 FSNP formulation to enable direct comparison.

SHSs	RMS height R_a (μm)	Autocorrelation length λ (μm)	Wenzel roughness	Contact angle hysteresis $\mathscr{H}$
v0	3.02 ± 0.71	7.81 ± 2.21	1.65 ± 0.05	1.37 ± 0.60
v1	4.34 ± 1.06	10.07 ± 3.48	1.83 ± 0.08	1.60 ± 0.62
v2	4.86 ± 1.47	10.81 ± 2.95	2.09 ± 0.15	2.60 ± 0.85
v3	4.40 ± 0.65	11.39 ± 1.34	1.97 ± 0.07	0.63 ± 0.40
FPOSS	2.34 ± 0.57	9.98 ± 1.74	1.44 ± 0.06	1.63 ± 0.26

Table 1. Surface roughness and wettability parameters for the tested SHSs.

First, the skin-friction performance of the various superhydrophobic surfaces (SHSs) was characterized in a fully developed turbulent channel flow over flow velocities ranging from 1.3 to 5 m/s, using streamwise pressure-drop measurements. The experimental arrangement, shown in Figure 1, consists of the SHS mounted as the upper wall of the channel, while a hydrodynamically smooth stainless-steel plate as the lower wall. Owing to limitations in the spray-coating setup, the maximum coating length achievable on the stainless substrate was 72 cm, which is considerably shorter than the overall channel length. As a result, the upper wall was assembled in two segments, each approximately 56 ∼cm in length.

The channel configuration enables direct estimation of wall shear stress from pressure losses, a standard and reliable approach for quantifying skin friction in internal turbulent flows. The streamwise pressure gradient, dP/dx, was obtained using ten pressure taps distributed along the centerline of the SF3 side windows at axial positions of 20H, 30H, 50H, 70H, 84H, 98H, 112H, 126H, 140H, and 150H. Flow transition was triggered at the channel inlet using 50-grit sandpaper strips to ensure fully turbulent conditions downstream. For data analysis, only pressure measurements from taps located between 70H and 150H—well downstream of the trip region—were used to ensure fully developed flow. The volumetric flow rate, Q, was independently measured using a Siemens Sitrans FM MAG5100 electromagnetic flow meter. The Reynolds number based on channel height, Re_H, varied from 10,000 to 55,000 and was computed as:

$$Re_H = \frac{U_m H}{\upsilon} \tag{4}$$

where U_m is the mean streamwise velocity obtained from volumetric flow rate and verified through PIV, H is the channel height, and υ is the kinematic viscosity of water.

Drag reduction (DR) was quantified from the streamwise pressure drop using:

$$DR(\%) = 2 \times 100 \left[\frac{C_{f,smooth} - C_{f,SHS}}{C_{f,smooth}} \right] \tag{5}$$

where $C_{f,smooth}$ and $C_{f,SHS}$ are the skin friction coefficients for the smooth and SHS surfaces, respectively. The factor of two accounts for drag reduction on only one wall of the channel.

Skin-friction coefficients were determined from the measured streamwise pressure gradient, dP/dx, evaluated over a 0.5 m test section of a rectangular channel with dimensions 1.14 m (length) × 0.1 m (width) × 0.007 m (height). This measurement region was located 0.56 m downstream from the inlet, corresponding to approximately 80 hydraulic diameters, ensuring fully developed flow conditions. The channel height was nominally 7 mm, and this value was independently confirmed using both bore gauge measurements and particle image velocimetry (PIV). Wall shear stress τ_w, friction velocity u_τ, and skin friction coefficient were calculated as:

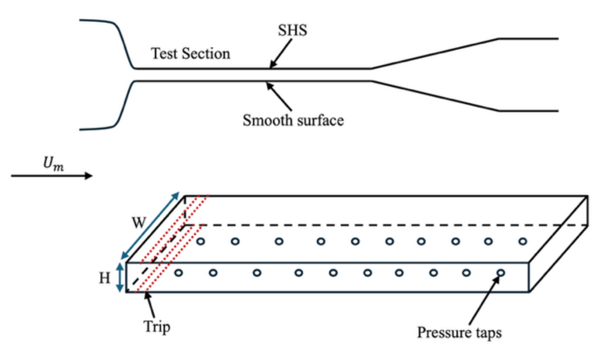

Figure 1. Schematic of the fully developed turbulent flow facility

$$\tau_w = -\frac{H}{2}\frac{dp}{dx} \tag{6}$$

$$C_f = \frac{\tau_w}{\frac{1}{2}\rho U_m^2} \tag{7}$$

$$u_\tau = \sqrt{\frac{\tau_w}{\rho}} \tag{8}$$

Frictional effects from the side walls were neglected due to their relatively small surface area.

In addition to channel flow measurements, the FSNP v2 and v3 surface was also evaluated in a developing turbulent boundary layer. These experiments were conducted in the Penn State Applied Research Laboratory (ARL) 12-inch closed-circuit water tunnel, which allows independent control of flow speed (0–24 m/s) and pressure (21–412 kPa). The tests were performed in a rectangular test section measuring 508 × 114 mm. A custom drag measurement system was installed through the bottom wall, consisting of a Kistler 9317C three-axis piezoelectric load cell mounted to a drag balance assembly. This setup directly measured the integrated hydrodynamic force acting on a flush-mounted test plate (146 mm × 311 mm), configured either as a smooth reference surface or coated with the SHS.

For baseline characterization, drag measurements on the smooth plate were repeated across the full operating speed range of the tunnel. Prior to each steady-state run, the flow was briefly reduced to reset the charge amplifiers connected to the load cell, minimizing long-term drift in the force signal. The tunnel was then accelerated to the target velocity, and after a stabilization period of 20–30 s, force data were acquired for 60 s at a sampling rate of 1000 Hz. Along with load-cell voltages, tunnel static pressure, velocity, and temperature were recorded, and the mean values at each condition were used to compute turbulent boundary-layer drag reduction over the Reynolds number range $Re_x = 10^6$–1.3×10^7, where x denotes the distance from the leading edge of the test plate:

$$DR_{TBL} = \frac{F_{smooth} - F_{SHS}}{F_{smooth}} \quad (9)$$

where F_{smooth} and F_{SHS} are the measured drag forces for the smooth plate and the SHS surface, respectively. This procedure was repeated over several months and multiple smooth-plate installations, yielding repeatability within 5

Results

Drag of spray-on SHSs The drag characteristics of several superhydrophobic coatings fabricated from fluorinated silica nanoparticles (FSNP) and fluorodecyl polyhedral oligomeric silsesquioxane (FPOSS) were measured in turbulent channel flow. Figure 2a presents the variation of the Drag Reduction (DR), with Re_H for the SHS surfaces in channel flow. Within our experimental range of Reynolds number, all coatings except NeverWet exhibited measurable drag reduction relative to the smooth baseline, with FSNP v2 and v3 showing the most pronounced performance. In comparison, FSNP v0, v1, and the FPOSS-based coating provided more modest reductions in skin friction.

FSNP v2 and v3 were produced at low spray pressure, which resulted in greater deposition of FSNP on the substrate and produced a broader distribution of surface roughness. In contrast, FSNP v0 and v1 were generated at higher spray pressures, leading to the formation of sharp, vertically oriented roughness features. When small droplets, representative of high-pressure condition of plastron, were placed on the surface, they readily rolled off v2 and v3 but remined pinned on v0 and v1. This behavior explains the performance of v2 and v3 under turbulent flow conditions. FPOSS coating also showed droplet pinning, suggesting possible plastron failure under high pressure.

All the tested drag-reducing surfaces show a clear dependence on Reynolds number, with higher drag reduction observed at lower Re_H (≈10000) and decline in performance as Re_H increases toward ≈40000. This reduction in effectiveness at higher Reynolds numbers is primarily associated with an increase in form drag arising from interaction between the flow and wetted surface asperities. At low Re, the viscous length scale (=υ/u_τ) is relatively larger than surface roughness, thereby damping out the roughness effects due to viscosity. As Re_H increases, viscous length scale becomes smaller, allowing roughness to extend beyond the viscous sublayer, which in turn increases the form drag. Consequently, we observed lower drag reduction at higher Reynolds numbers.

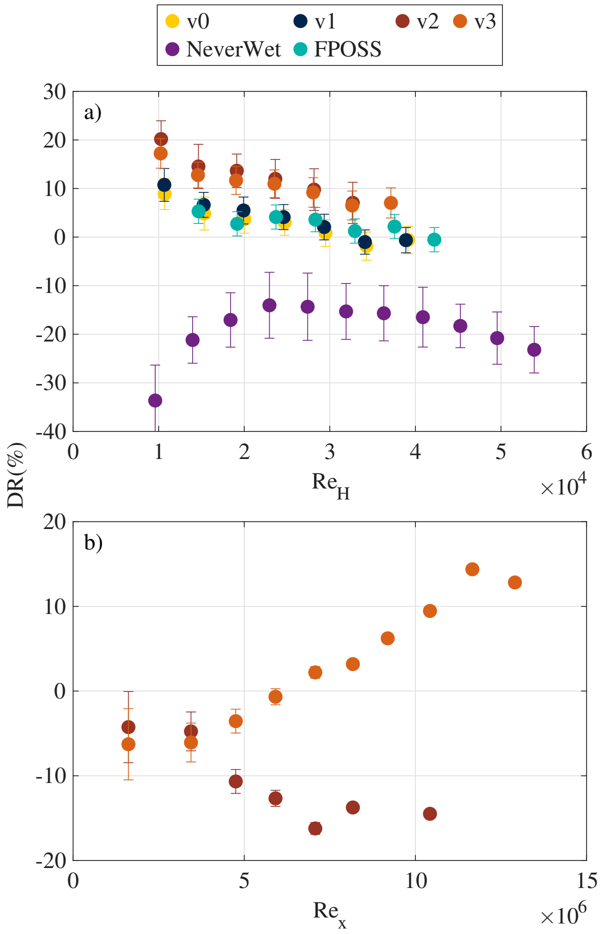

Figure 2. (a) Percentage drag reduction by all SHS in channel flow with Re_H (b) Percentage drag reduction by v2 and v3 with boundary layer flow with Re_x

Because of the strong drag-reduction performance observed for FSNP v2 and v3 in channel flow, these surfaces were further evaluated in a developing turbulent boundary layer in ARL 12-inch water tunnel. In this configuration, FSNP v2 exhibited an increase in drag relative to the smooth reference surface, in contrast to its behavior in channel flow where drag reduction was observed. On the other hand, FSNP v3 consistently produced substantial drag reduction, reaching approximately 15% even at high Reynolds number ($Re_x = 1.2 \times 10^7$). Notably, unlike the channel flow results where drag reduction decreased with increasing Reynolds number, the boundary layer measurements showed an increase in drag-reduction magnitude with increasing Re_x. This contrasting behavior suggests that additional flow physics and surface–flow interactions may play a role in the boundary layer configuration, proposing further investigation.

Longevity of drag reduction Superhydrophobic surfaces in water often experience a gradual decline in performance due to depletion of the plastron (entrapped air layer), as reported by Gose *et al.* (2018). Therefore, beyond achieving high drag reduction, it is equally important for a surface to maintain its effectiveness over extended durations. To assess the long-term stability of the present surface, a 10-hour longevity study was conducted on FSNP v2 at Reynolds numbers of Re_H = 14,500, 23,500, and 37,200 in channel flow. In all cases, the measured skin friction remained nearly constant throughout the experiments, indicating effective retention of the plastron layer. In addition, FSNP V2 was evaluated in a boundary layer flow at $Re_x \approx 10^7$ for 3 hours, during which the surface consistently sustained its drag reduction performance.

Effect of mean pressure level Drag reduction over superhydrophobic surfaces (SHSs) is primarily attributed to the effective slip generated by a stable plastron layer. However, variations in hydraulic pressure can alter the liquid–air interface and consequently influence drag-reduction performance. To investigate these effects, experiments were performed in turbulent channel flow and boundary layer flow over a range of hydraulic pressures and Reynolds numbers. Sample v3 was selected for this study because it exhibited the highest drag reduction at high Reynolds numbers. Measurements were conducted at pressure conditions of $\phi = p/p_{atm}$ = 0.82, 1 (atmospheric), and 1.18 in channel flow, as well as 1 and 1.26 in boundary layer flow. The corresponding drag-reduction results are presented in Figure 3. High pressure still shows the drag reduction while at low pressure, there is significant increase in drag.

The observed behavior may be explained by two possible mechanisms. The first is associated with pressure-dependent changes in the plastron thickness and stability. When the external pressure is increased, the entrapped air layer becomes compressed, while the surrounding water tends toward an undersaturated state, promoting gradual gas dissolution into the liquid. Although this process may slightly reduce the plastron thickness, the applied overpressure of ϕ =1.18 and 1.26 does not appear large enough to significantly affect the stability of the air layer, allowing the drag-reduction performance to remain essentially unchanged. Under reduced pressure conditions (ϕ = 0.82), the situation differs substantially. The surrounding water becomes supersaturated, which promotes gas release and expansion of the plastron. The resulting thicker air layer may also become less stable and more deformable. Instead of acting as a stable slip surface, the expanded plastron may behave more like a compliant interface, which can enhance flow disturbances and ultimately increase drag.

A second explanation may arise from capillary effects at the liquid–air interface. Lower ambient pressure decreases the capillary restoring force that resists interface deformation, making the plastron more vulnerable to turbulent fluctuations. Increased interface deformation, or intermittent rupture of the plastron, could therefore contribute to the measured drag increase. Further investigation is needed to determine the relative importance of these mechanisms and to better understand the governing physics.

Effect of water saturation levels As discussed previously, variations in ambient pressure can influence the concentration of dissolved gases in water, which may subsequently affect the properties of the plastron layer. To further investigate the influence of dissolved oxygen (DO) on plastron stability, experiments were conducted using surface v3 in turbulent channel flow at a reduced DO concentration of 30%, under the same three pressure conditions considered earlier: ϕ = 0.82, 1 (atmospheric), and 1.18.

The experimental results show that, at this lower DO concentration, the drag reduction becomes largely insensitive to the applied pressure (Figure 4). This behavior is likely associated with thinning of the plastron layer at reduced dissolved oxygen levels, which decreases the sensitivity of the interface to additional pressure-induced changes. As a result, variations

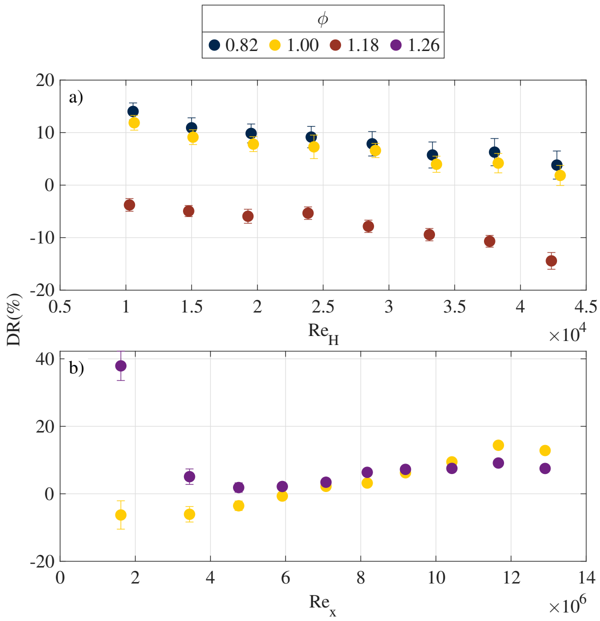

Figure 3. Percentage drag reduction by FSNP v3 substrate under (a) $\phi = p/p_{atm}$ = 0.82, 1 (atmospheric), and 1.18 in channel flow (b) ϕ = 1.26 in boundary layer flow

in pressure did not produce any statistically significant change in either the plastron characteristics or the measured drag reduction.

Moreover, as shown in Figure 4, the plastron became thinner at low DO levels, which corresponded to a decrease in drag reduction. This may have been caused by an increase in form drag resulting from greater surface roughness.

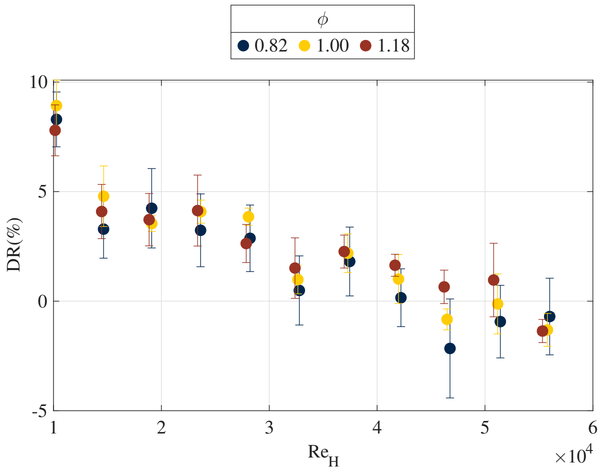

Figure 4. Percentage drag reduction by FSNP v3 substrate under $\phi = p/p_{atm}$ = 0.82, 1 (atmospheric), and 1.18 and 30% DO level

Summary and Conclusions

This study shows that spray-on superhydrophobic surfaces (SHSs) can achieve measurable and, in some cases, sustained skin-friction drag reduction in turbulent flows, highlighting their potential for marine applications. Among the tested coatings, FSNP-based surfaces - particularly v2 and v3 - performed best due to their ability to maintain a stable plastron and support effective interfacial slip. In channel flow, drag reduction decreased with increasing Reynolds number, mainly because of growing roughness-induced form drag. In contrast, boundary layer tests showed that FSNP v3 maintained strong performance, achieving up to 15% drag reduction at high speeds, while v2 transitioned to drag increase. Unlike channel flow, the boundary layer results showed an overall increase in drag reduction with Reynolds number for v3, indicating a strong influence of flow configuration on SHS behavior. Longevity tests further confirmed surface robustness. FSNP v2 maintained nearly constant skin friction over 10 hours in channel flow and sustained performance for 3 hours in boundary layer flow without noticeable degradation, indicating good plastron stability under continuous operation. Pressure and dissolved gas effects also played an important role in the observed drag reduction. While ϕ =1.18 had minimal impact, ϕ = 0.82 increased drag due to reduced plastron stability and enhanced interface deformation. However, at reduced dissolved oxygen levels (30%), drag reduction became largely insensitive to pressure, suggesting a thinner but less responsive plastron, with drag increases mainly linked to form drag from surface roughness.

Overall, SHS performance is governed by coupled effects of surface morphology, plastron stability, pressure, and gas content. The combined channel and boundary layer flow experiments demonstrate that durable drag reduction is achievable, but its magnitude and stability strongly depend on operating conditions, motivating further studies under more realistic marine flow environments.

ACKNOWLEDGEMENT

This work is supported by DARPA with Dr. Susan Swithenbank and Dr. Keith Whitener, Program Managers, under DARPA contract HR00112490349 (Phase 2). We would also like to acknowledge Prof. Gareth McKinley, Prof. Krishnan Mahesh and their research teams for their valuable contribution.

REFERENCES

Bushnell, D. M. & Moore, K. J. 1991 Drag reduction in nature. *Annual Review of Fluid Mechanics* **23**, 65–79.

Ceccio, Steven L. 2010 Friction drag reduction of external flows with bubble and gas injection. *Annual Review of Fluid Mechanics* **42**, 183–203.

Choi, K.–S., Yang, X., Clayton, B. R., Glover, E. J., Atlar, M., Semenov, B. N. & Kulik, V. M. 1997 Turbulent drag reduction using compliant surfaces. *Proceedings of the Royal Society of London. Series A: Mathematical, Physical and Engineering Sciences* **453**, 2229–2240.

Ems, Henry, Tsubaki, Alfred, Sukup, Ben, Nejati, Siamak, Alexander, Dennis, Zuhlke, Craig & Gogos, George 2021 Drag reduction in minichannel laminar flow past superhydrophobic surfaces. *Physics of Fluids* **33**.

Golovin, Kevin B., Gose, James W., Perlin, Marc, Ceccio, Steven L. & Tuteja, Anish 2016 Bioinspired surfaces for turbulent drag reduction. *Philosophical Transactions of the Royal Society A: Mathematical, Physical and Engineering Sciences* **374**, 20160189.

Gose, James W., Golovin, Kevin, Boban, Mathew, Mabry, Joseph M., Tuteja, Anish, Perlin, Marc & Ceccio, Steven L. 2018 Characterization of superhydrophobic surfaces for drag reduction in turbulent flow. *Journal of Fluid Mechanics* **845**, 560–580.

KAMETANI, YUKINORI & FUKAGATA, KOJI 2011 Direct numerical simulation of spatially developing turbulent boundary layers with uniform blowing or suction. *Journal of Fluid Mechanics* **681**, 154–172.

Kang, Sangmo & Choi, Haecheon 2000 Active wall motions for skin-friction drag reduction. *Physics of Fluids* **12**, 3301–3304.

Li, Zexiang, Liu, Xiaochao, Lv, Pengyu & Feng, Yi 2022 Drag reduction of blowing-based active control in a turbulent boundary layer. *Physics of Fluids* **34**.

Mei, C. C. & Guo, X. Y. 2018 Numerical study of laminar boundary-layer flows over a superhydrophobic plate. *Physics of Fluids* **30**.

Min, Taegee & Kim, John 2004 Effects of hydrophobic surface on skin-friction drag. *Physics of Fluids* **16**, L55–L58.

Park, Hyungmin, Choi, Chang-Hwan & Kim, Chang-Jin 2021 Superhydrophobic drag reduction in turbulent flows: a critical review. *Experiments in Fluids* **62**, 229.

Rastegari, Ehsan & Graham, Michael D. 2018 Turbulent skin-friction drag reduction with superhydrophobic longitudinal microgrooves and riblets. *Journal of Fluid Mechanics* **834**, 514–537.

Rothstein, Jonathan P. 2010 Slip on superhydrophobic surfaces. *Annual Review of Fluid Mechanics* **42**, 89–109.

SANDERS, WENDY C., WINKEL, ERIC S., DOWLING, DAVID R., PERLIN, MARC & CECCIO, STEVEN L. 2006 Bubble friction drag reduction in a high-reynolds-number flat-plate turbulent boundary layer. *Journal of Fluid Mechanics* **552**, 353–380.

Tomlinson, Samuel D., Gibou, Frédéric, Luzzatto-Fegiz, Paolo, Temprano-Coleto, Fernando, Jensen, Oliver E. & Landel, Julien R. 2023 Laminar drag reduction in surfactant-contaminated superhydrophobic channels. *Journal of Fluid Mechanics* **963**, A10.

Zheng, Borui, Lin, Deling, Qi, Shaojie, Hu, Yuzhe, Jin, Yuanzhong, Chen, Quanlong, Bian, Dongliang & Yan, Rihua 2023 Turbulent skin-friction drag reduction by annular dielectric barrier discharge plasma actuator. *Physics of Fluids* **35**.